respectively. Both types of tilt-sensors; SSC and SA were setup on the slope surface and slope top as shown in Fig. 1 where distances and numbering of sensors are also done. There are four SSC (SSC1, SSC2, SSC3 and SSC4) and five SA (SA1, SA2, SA3, SA4 and SA5) tilt-sensors. The slope surface is divided into 10 equal widths so that each excavation (cut) width is equal to 0.5 m. Excavation is started from the toe of the slope, vertically downward using a backhoe. Therefore, the height of excavation in each cut increases by 0.5 m. Five minutes waiting time was allowed after each cut. Cutting of slope was done until the slope failure occurred. Here, total of 6 cuts were done. Some partial failure within the slope was observed after 5th cut. But the final large failure was observed after 6th cut, failure reaching up to the slope crest.

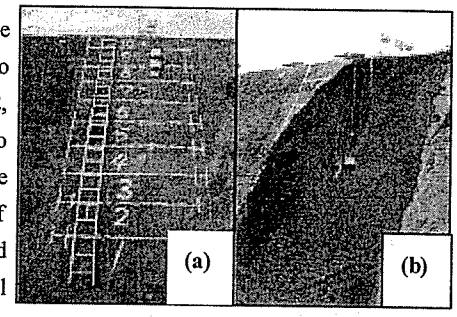

Photo. 3 (a) Before cut and (b) after failure

3. Test Results

Photo 3 shows the model slope before the starting of the cut and after the failure. Cracks were also seen before failure on the slope top. Figures 2 and 3 show the movement of SSC and SA tilt-sensors measured along X and Y directions. Movement of the whole slope could be made by comparing the X and Y movements. In the figures, solid vertical lines represent the number of cut and dashed line in between the solid lines represents occurrence of partial failure whereas the dashed line at the end represents the final failure. Although it is difficult to see the amount of movement for the first few cuts, increment in the slope movement with the progress of cut could be seen in all the sensors. In all the figures, sharp increment in the movement after 5th and 6th cuts could be seen. Partial failure was observed after 5th cut (at 48 min.) and final large failure was observed after 6th cut. Just before the occurrence of both failures, sharp increment in the tilt angle could be seen in all the cases, especially SSC 1, 2 and SA 1, 3. Since the trend of failure pattern could be clearly measured using these tilt-sensors, practical application of these sensors in the real excavation field is possible. Comparing the ranges of movements (tilt angle) measured by SSC and SA placed at the same positions, it was found that their difference is very less which shows that both types of tilt-sensors are equally applicable in the field.

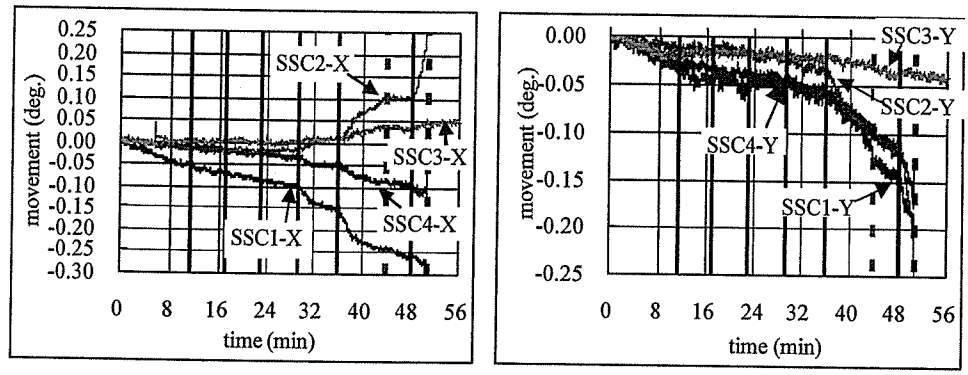

Fig. 2 Movement of slope surface and slope top measured from Small Size Compact Tilt-sensor

4. Conclusions

(1) Both types of tilt-sensors could measure the slope movement during the excavation. In addition, prominent and sharp movement of the slopes just before the failure could also be measured which shows the possible application of these tilt-sensors in the slope excavating field. (2) Measured amount of movement of tilt angle at the same position by SSC and SA tilt-sensors are almost same. This suggests that both types of tilt sensors could be used with equal preference.

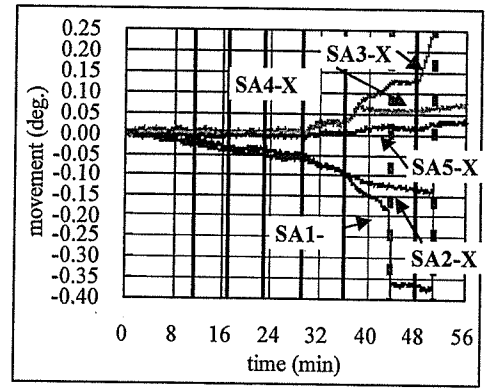

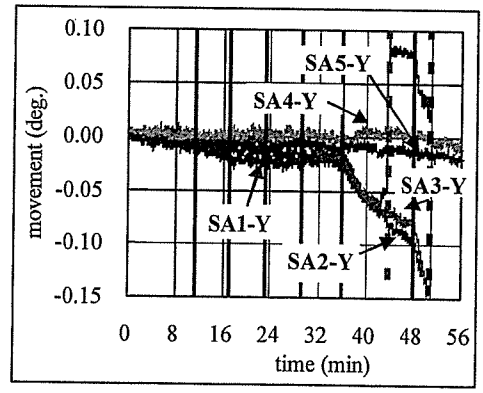

Fig. 3 Movement of slope surface and slope top measured from Stand Alone Tilt-sensor

5. Acknowledgement

This work is partially carried out under the Health and Labor Sciences Research Grants of Ministry of Health, Labor and Welfare.

References

Takemoto, M., Satou A., Matsuyma H., Ogata K., Kunimi T., Ito S. and Nezu M, 2001, "*Development of new In-place inclinometer in bore using accelerate sensor*", 36th Annual meeting of Japanese Geotechnical Society, pp. 179~180 (in Japanese).

切土掘削工事中の斜面崩壊機構に関する実物大実験～試料の違いによる影響について～

武蔵工業大学大学院　学○小板橋拓馬　正　末政直晃
(独)労働安全衛生総合研究所　正　伊藤和也　Tamrakar S.B　豊澤康男
(株)技研製作所(元　武蔵工業大学大学院)　正　日下部　澄音

1.はじめに

道路拡幅工事や急傾斜地対策工事では、従来よりも斜面の勾配を急にし、そこに重力壁等を設置し斜面を安定にすることが多くある。これらの構造物は最終的には斜面を安定化させることができるが、その設置過程においては斜面が不安定化し、崩壊に至ることがある。このような災害を防ぐためには、切土掘削工事における斜面崩壊機構を解明し、廉価で経費に余裕のない中小規模工事でも利用可能な計測施工技術や安全な対策方法の提案が必要である。本報告では、2 種類の試料（成田砂、関東ローム）を用いた盛土斜面の法尻部からの切土掘削による実物大斜面崩壊実験の結果について示す。そこで、両実験を比較することで、異なった試料における斜面崩壊現象の違いについて考察する。

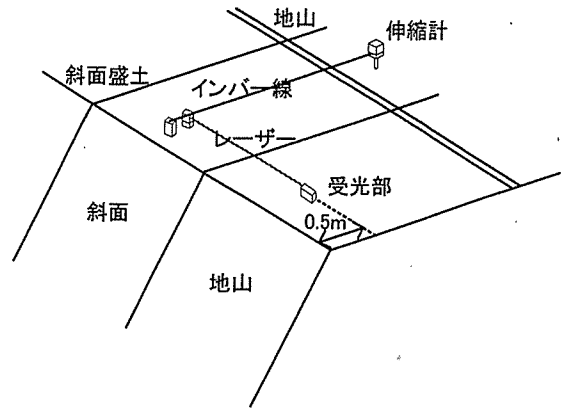

図-1　計測器設置位置

2実物大実験

2.1施工概要

盛土斜面による実物大実験は、大型宅地造成地域内において、高さ5m、斜面角度50° に切り取った地山（関東ローム）を本体構造とし、腹付盛土形式で、高さ5m、斜面角度45°の斜面を築造して行った。実験に使用した盛土材料は、現地発生土である関東ロームと成田砂である。これら2種類の試料について、転圧回数を0回、5回とそれぞれ変化させ、幅3.5mとなる4種類の試験盛土を作製した。本報ではそのうちの転圧0回の結果について報告する。作製された盛土に対して原位置試験（スウェーデン式サウンディング試験、簡易動的コーン貫入試験）を行った。その詳細については文献[1]が詳しいが、成田砂では深さに比例して強度が発現しているのに対して、関東ロームではほぼ一定強度となっており、地盤材料の特徴がよく見られる結果となっている。

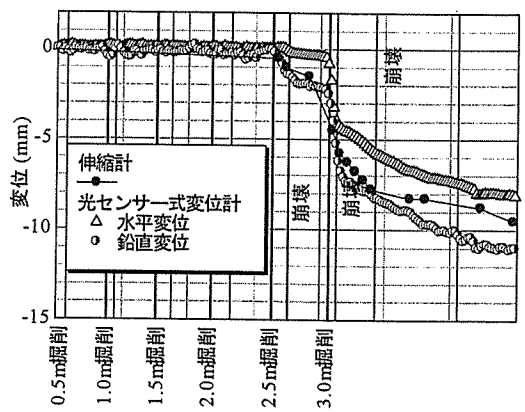

部分的な崩壊

図-2 掘削段階での各種計測器の挙動と崩壊状況(成田砂)

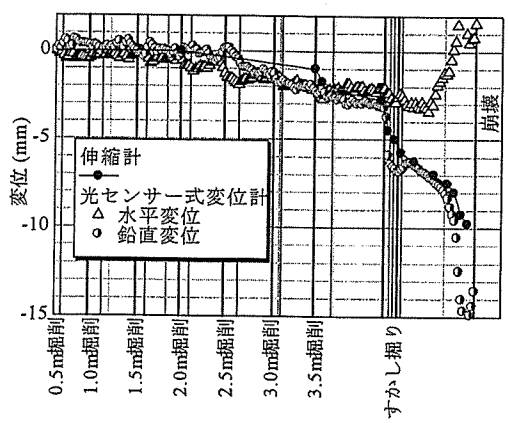

すかし掘りによる崩壊

図-3 掘削段階での各種計測器の挙動と崩壊状況(関東ローム)

キーワード　斜面安定，労働災害，掘削
連絡先　〒158-8557　東京都世田谷区玉堤 1-28-1　武蔵工業大学　地盤環境工学研究室　TEL 03-5707-2202

2.2実験概要

斜面の切り取りは、バックホーを用いて行った。掘削方法は1回の切り取り高さを約0.5m、掘削幅約2.5mとし、1回の掘削終了後、約5分間放置した。掘削は、崩壊するまで行うが、計測器の都合上、最大で7回（高さ約3.5m）までとした。地盤変形挙動を把握するため、法面天端の変位をワイヤー式伸縮計（以下、伸縮計）およびレーザー光と光センサーによる2次元変位計[2)]（以下、光センサー式変位計）を図-1に示す位置に設置して計測した。

2.3実験結果と考察

図-2に成田砂、図-3に関東ロームの光センサー式変位計による鉛直・水平変位、そして伸縮計による変位の経時変化を代表的な崩壊状況とともに示す。まず、成田砂は、切り取り高さ2.5mまで変位が見られなかった。しかし、2.5m掘削中から徐々に変形し、伸縮計と光センサー式変位計の鉛直方向に約2mm変位した際、その放置時間中に斜面内にて部分的な崩壊が生じた（図-2 写真参照）。その後、さらに切り取り高さ3.0m掘削中から、水平変位とともに緩やかに変位が始まり、鉛直変位が8mm程度変位した際、片側の側面を含めた崩壊が生じた。関東ロームは、2.5m掘削中から光センサー式変位計による水平・鉛直変位、伸縮計にて変位が計測されたが、成田砂で崩壊が生じた変位量（2mm）に達しても崩壊に至らず、結果的に、通常の掘削段階では崩壊は生じなかった。そのため、下段部分を掘削してオーバーハング状態にする“すかし掘り”を行ったところ、光センサー式変位計による鉛直方向に15mm、伸縮計に10mm程度変位した際、天端部分から大規模な崩壊が生じた（図-3 写真参照）。経時変化については上述のようであるが、水平方向と鉛直方向の変形について地盤条件の違いが与える影響を確認するために、図-4～5に水平変位と鉛直変位の関係をそれぞれ示す。まず、成田砂では、3回の崩壊が発生している。その中でも法面内にて発生した崩壊直前の挙動は、鉛直変位が沈下し、水平変位が変化していない状態にて発生している。その後の2回の崩壊直前の挙動は、水平・鉛直変位ともに急激な挙動を数mm程度示していることが分かる。労働災害が発生するような斜面崩壊は、最初に発生するような法面内崩壊によるものが多いため、この崩壊直前の挙動を把握することは重要だと考えられる。一方、関東ロームでは、通常の掘削段階では崩壊が生じなかったが、特徴的な変位挙動は見られなかった。また、すかし掘り後での崩壊直前の挙動は、成田砂の法面内崩壊直前と同様に、その変位量は鉛直方向が卓越している。以上のことから地盤材料の違いにより変形挙動に大きな差があることが分かった。

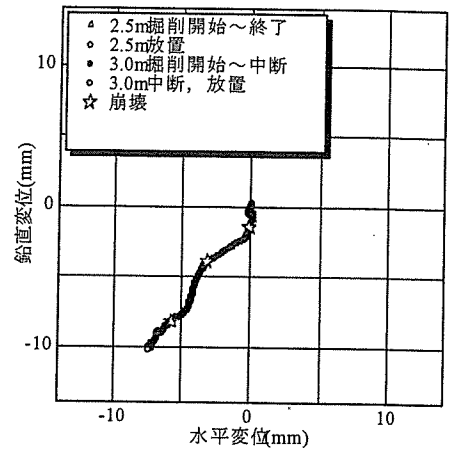

図-4 水平・鉛直変位の挙動(成田砂)

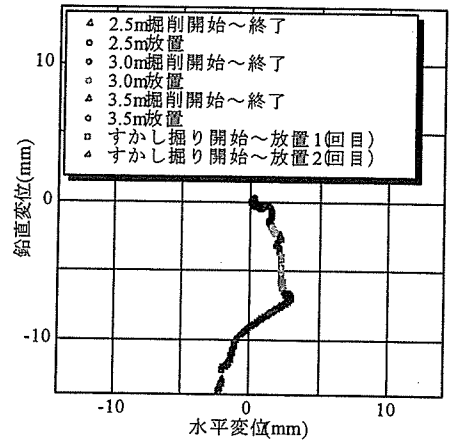

図-5 水平・鉛直変位の挙動(関東ローム)

3.まとめ

盛土築造斜面による実物大実験を行い、掘削に伴う斜面崩壊現象の把握および異なった試料における斜面崩壊現象の違いについて考察を行った。その結果、以下の知見を得た。

1. 崩壊直前の変位量は約8mm（成田砂）、15mm（関東ローム）であり微小変位ではあるが計測することが出来た。このことから、斜面を計測することによって崩壊の事前予測も可能であると考えられる。
2. 光センサー式変位計から得られた掘削段階初期での水平・鉛直変位に着目したところ、成田砂では鉛直方向に沈下したのに対して、関東ロームでは、ほとんど動きが見られなかった。また、崩壊直前の挙動は、掘削方法にかかわらず、両者とも鉛直方向に変位が生じた際に発生した。

なお、本研究では法肩部のみに計測器を設置しているが、設置位置により傾向は異なることも考えられる。そのため、計測器の最適な設置位置についても今後検討しく予定である。

参考文献 1)堀井ら：切土掘削工事中の斜面崩壊機構に関する実物大実験（その1～実験概要）、第41回地盤工学研究発表会、投稿中 2)伊藤ら：「レーザー光と光センサーを利用した土砂崩壊検知システムの開発～複眼タイプによる2次元変位計測～」、第41回地盤工学研究発表会、投稿中

Comparison of slope failure trend just before failure in the field using newly developed tilt-sensor

Japan National Institute of Occupations Safety and Health Regular member O Tamrakar S. B.
Japan National Institute of Occupations Safety and Health Regular member Toyosawa Y. and Itoh K.
Akebono Brake Industry Co. Ltd. Non-member Kunimi T., Nishijyo A. and Okubo T.

1. Introduction

Tamrakar et al. (2006) have developed a new type of tilt-sensor which could be used to measure the movement of the slope just before the failure in terms of tilting angle. They had tested its application in the field with Narita sand embankment model using Small Size Compact (SSC) and large size Stand Alone (SA) type tilt-sensors. In this report, comparison of tilt angle measured from SSC and SA type Tilt-sensors for two different types of soil embankments (Narita sand and Kanto loam) are made and their failure pattern are discussed.

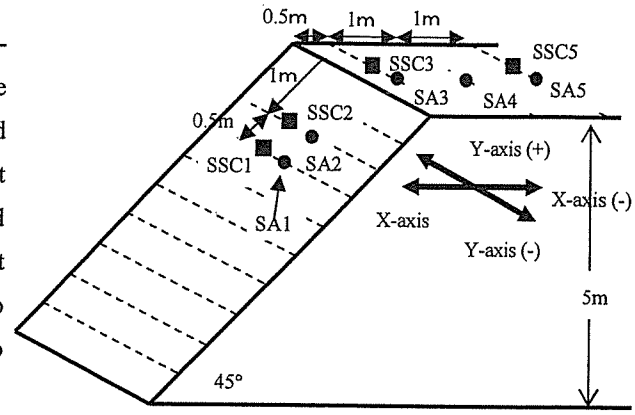

Fig. 1 Layout of tilt-sensors set up

2. Tilt- sensor and Field Test

Directions of movement of tilt-sensor (Tamrakar et. al, 2006) are shown in Fig. 1 and Photo 1. Four SSC (SSC1, SSC2, SSC3 and SSC5) and five SA (SA1, SA2, SA3 SA4 and SA5) tilt-sensors were set up on the slope surface and slope top (Fig. 1). Water content and wet density of Narita sand slope model and Kanto loam slope model obtained from sand replacement technique in the field were 1.74g/cm^3 and 29.3% and 1.18g/cm^3 and w=111.3%, respectively. Each model slope is of 5m height, 3.5 width and 45 degree slope angle. Slope surface was divided into 10 equal widths, each with 0.5 m. Excavation is started from the toe of the slope, vertically downward using a backhoe. Five minutes interval was allowed after each cut to see the failure trend. Cutting of slope was continued until the slope failure occurred. In case of Narita sand total of 6 cuts were made. Some partial failure within the slope was observed after the 5th cut. But the final large failure was occurred after 6th cut (around 51 min. elapsed time) which reached up to the slope crest. For Kanto loam, altogether 9 cuts were made. First partial failure was occurred after 8 cut (78 min. elapse time) at the right side of the slope (right wall). Large change in tilt angle could during this partial failure was stopped around 88 min. Further excavation on the left side of the slope was made so that final failure was occurred which reached up to SA3 (SSC3) position on the slope crest.

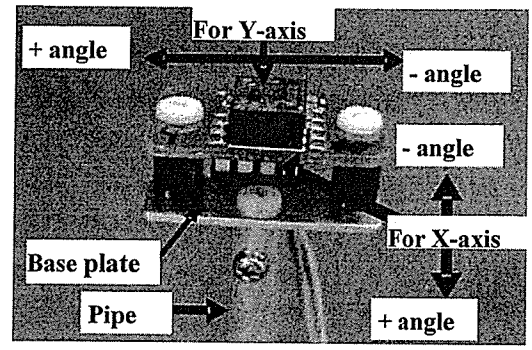

Photo 1 SSC-tilt-sensor

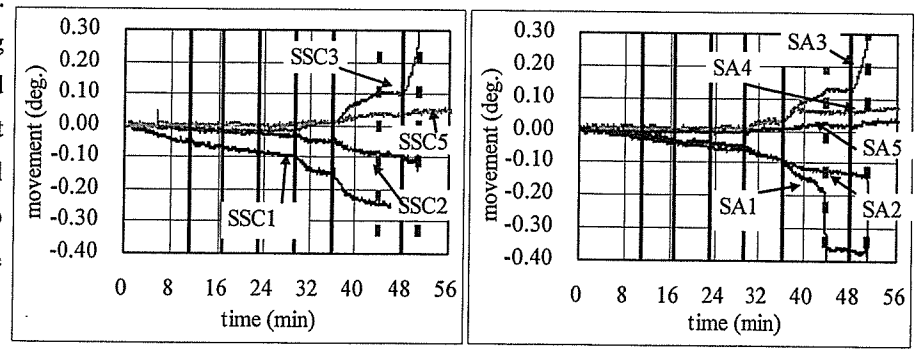

Fig. 2 Movements measured from SSC and SA Tilt-sensors (X-axis) for Narita sand

Keywords: **Monitoring on site/measurement, Slope, Excavation**
National Institute of Industrial Safety, JNIOSH, Construction Safety Division,
1-4-6 Umezono, Kiyose-Shi, Tokyo-204-0024. Tel: 042-491-4512, Fax: 042-494-6214, Email:tamrakar@s.jniosh.go.jp

3. Test Results

Movement of slope with SSC and SA tilt-sensors along X-direction for Narita sand and Kanto loam are shown in Figs. 2 and 3 (only X-direction is shown). Solid thick vertical lines in the graph show the end of excavation steps. Dotted lines in between these lines show the occurrence of partial failure where as the last thick dotted line shows occurrence of final failure. Sudden change in the tilt angles was seen just before the partial and final failures in both types of tilt–sensors. Kanto loam showed larger movement and took longer time to fail than that by Narita sand despite of wet density of Narita sand being higher than that of Kanto loam. Comparing the movements of SSC and SA for each soil, similar pattern of failure movement could be seen. In case Narita sand, SSC1, SSC2, SA1 and SA2 showed negative values while SSC3, SSC5, SA3, SA4 and SA5 showed positive value. Negative values shows the backward and downward movement of slope while the upper tilt sensors placed on the slope top showed the forward and downward movement of slope (Fig. 4(a). This shows the movement of slope during partial and final failure in different directions. In case of Kanto loam also similar movements of SSA and SC tilt-sensors were seen. Here, all the sensors moved forward and downward, showing partial and final movement taking in the same direction (Fig. 4(b)). Change in the tilt angle for each tilt-sensor along X-direction at particular elapsed time for each soil type is shown in Table 1. Comparing the amount of change in the tilt angle, it was seen that both types of tilt-sensors show almost same values except SSC2, SA2, SSC5 and SA5. This shows the application of both types of tilt-sensors with equal efficiency in the field.

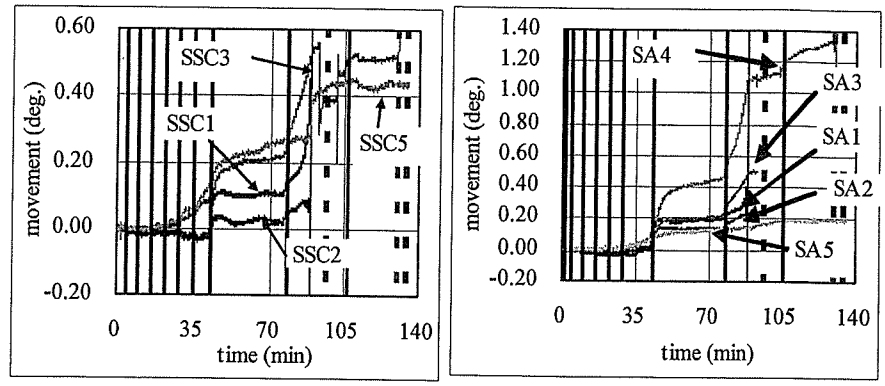

Fig. 3 Movements measured from SSC and SA Tilt-sensor (X-axis) for Kanto loam

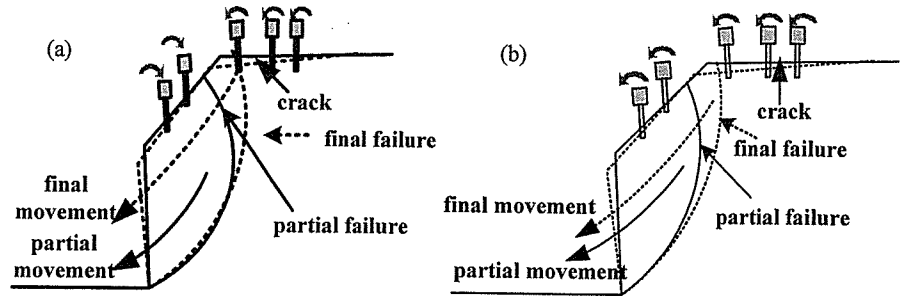

Fig. 4 Failure pattern in two types of soil models (a) Narita sand and (b) Kanto loam

Table 1 Comparison of tilt-angles measured

Narita sand (around 51 min. elapsed time)					
tilt-angle (X-axis)	1	2	3	4	5
SSC	-0.275	-0.11	0.25	-	0.025
SA	-0.300	-0.15	0.25	0.06	0.025
Kanto loam (around 88 min. elapsed time)					
tilt-angle (X-axis)	1	2	3	4	5
SSC	0.50	0.08	0.54	-	0.400
SA	0.50	0.30	0.50	1.08	0.150

4. Conclusions

1). Sudden movement just before failure could be seen in both types of tilt-sensors. Both SSC and SA tilt-sensors show almost same pattern and same amount of movement for particular soil model. This shows the application of both types of tilt-sensors in the field with equal efficiency. 2). Failure pattern of different soil could be measured with this new type of tilt-sensor. In case of Narita sand, partial and final failure directions are different whereas for Kanto loam, they are same.

Acknowledgement

This work is partially carried out under the Health and Labor Sciences Research Grants of Ministry of Health, Labor and Welfare.

References

Tamrakar, S.B., Toyosawa, Y., Itho, K., Kunimi T., Nishijo A. and Okubo S., 2006, "Development of Tilt-sensor and possibility of measurement of failure trend just before the failure", 41th Annual meeting of Japanese Geotechnical Society (under print)

Deformation Characteristics of Sandy Clay during Slope Excavation

Japan National Institute of Occupational Safety and Health Regular member ○Timpong Sahaphol
Japan National Institute of Occupational Safety and Health Regular member Tamrakar S. B.
Japan National Institute of Occupational Safety and Health Regular member Toyosawa Yasuo
Japan National Institute of Occupational Safety and Health Regular member Itoh Kazuya

1. Introduction

Centrifuge modeling in combination with a digital image analysis technique was performed to evaluate two-deformational displacements such as maximum shear strain distribution of sandy clay soil during the slope excavation. The centrifuge test was conducted using the Mark-II centrifuge at the Japan National Institute of Occupational Safety and Health, which is capable of simulating both of dynamic and static geotechnical problems.

2. Model preparation

The model test was performed in a rigid model box with transparent Plexiglas sidewall to enable side viewing of the model during centrifuge flight. The internal dimensions of the rectangular model box are 150×450×272 mm. The sandy clay ground model was prepared by mixing Toyoura sand and Kaolin (NSF clay) as a ratio of 3:1 by weight at 10 % water content. The mixture was then placed into the model box and compacted in 13 layers (20 mm thickness per layer) under a pressure of 50 kPa by the bellofram cylinder. The unit weight after the compaction was about 15 kN/m^3. The resulting block of ground model was trimmed to form the slope geometry. Figure 1 shows a schematic view of the experimental model and arrangement of linear variable displacement transducers (LVDTs). In order to observe the deformations of the slope during centrifuge test, a grid-printed membrane was set between the transparent sidewall and the ground model. The friction between the sidewall and the membrane was reduced by smearing the sidewall surface with silicon grease. The digital video and CCD cameras were mounted directly in front of the model box, which is capable of providing a continuous record during testing. The resolution and physical size of the image acquired by the CCD camera was 1600×1200 and 560×420 mm, respectively, thus the resolution is approximately 0.35 mm per pixel.

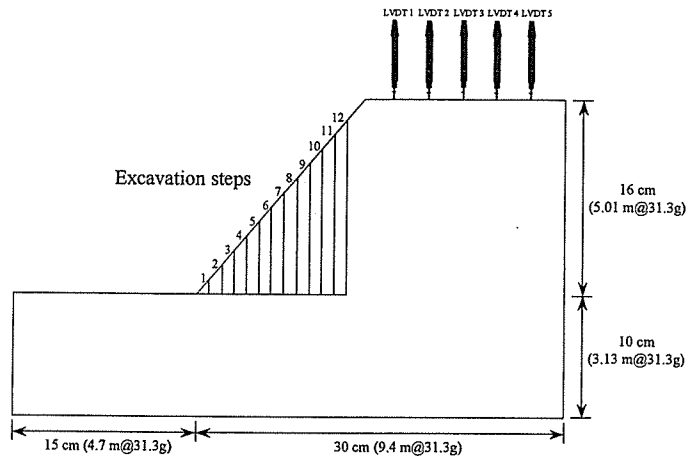

Fig. 1. The experimental slope model

3. Simulation of slope excavation

After the model box was loaded onto the centrifuge payload platform, the centrifuge acceleration level was gradually increased in steps of 5g after there was no variation in surface settlement observed from the displacement transducers. The in-flight slope excavation was conducted at the centrifuge acceleration of about 31.3g where the height of slope was 5 m corresponding to the prototype scale. The NIIS in-flight excavator, which can excavate the model ground vertically during the high centrifuge acceleration environment, was used in this paper for simulating the slope excavation process. The detail of the NIIS in-flight excavator was described by Toyosawa et al. (1998). The movement of the in-flight excavator was controlled manually from the computer room, the slope model was excavated step by step as shown in the Fig. 1 until the failure of slope can be observed.

Keywords: image analysis, centrifuge, slope excavation

204-0024, Tokyo, Kiyose, Umezono, Japan National Institute of Occupational Safety and Health, Tel 04-2491-4512 (Ext. 432)

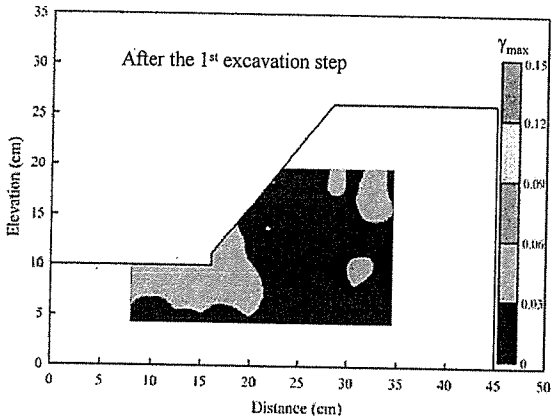

Fig. 2. Distribution of γ_{max} after the 1st excavation

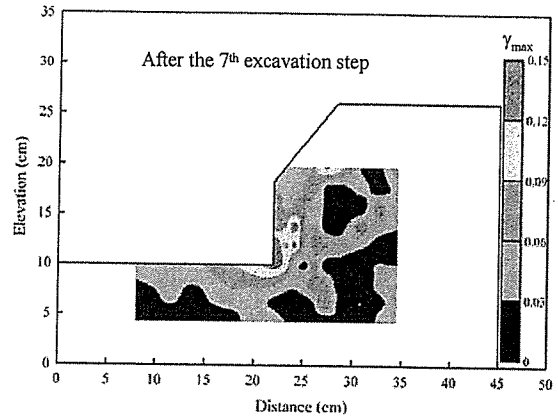

Fig. 4. Distribution of γ_{max} after the 7th excavation

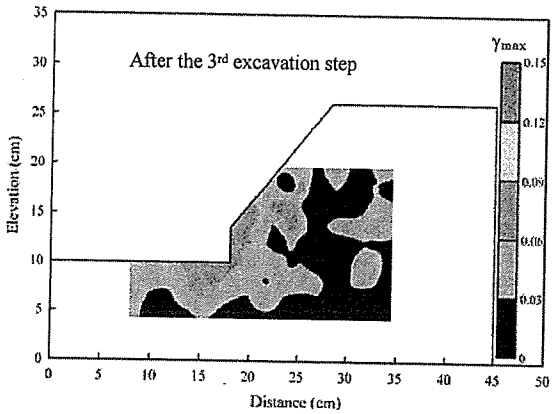

Fig. 3. Distribution of γ_{max} after the 3rd excavation

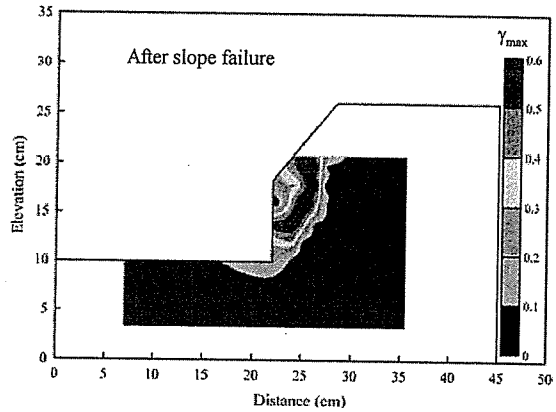

Fig. 5. Distribution of γ_{max} just after the failure

4. Test results

The failure of slope was clearly observed after the 7th excavation step. The two-dimensional deformations of the ground model can be evaluated by measuring the displacements of grid-printed membrane captured by taking photographs after each step of the in-flight excavations. Each rectangular grid was divided into two triangles, and the Lagrangian strains on these two triangles were averaged and then used to compute the engineering strain. Figures 2 to 5 show the distribution of the maximum shear strain ($\gamma_{max} = \varepsilon_1 - \varepsilon_3$) after the 1st, 3rd, 7th excavation steps and just after slope failure, respectively. It should be noted that the separations of the maximum shear strain contours in the figures were due to the limited boundaries of the Plexiglas sidewall where the targets outside the Plexiglas sidewall cannot be identified. As can be seen in the figures, after each excavation step the progressive failure can be observed from the toe toward to the upper part of the slope. Figure 6 shows the photograph of the slope failure, the observed failure plane was found in good agreement with the distribution of the maximum shear strain.

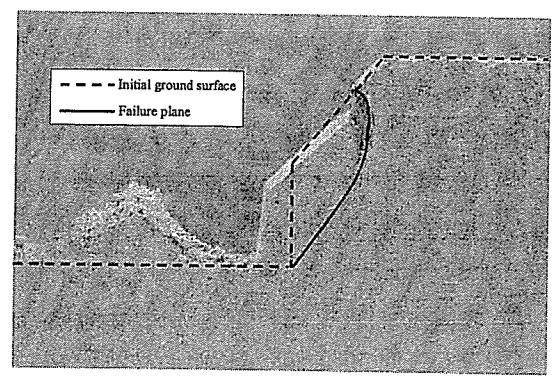

Fig. 6. The location of failure plane

5. Conclusions

The centrifuge modeling in combination with the digital image analysis made it possible to evaluate quantitatively the two-dimensional deformation characteristics of sandy clay soil during the slope excavation.

Reference

Toyosawa, Y., Horii, N., and Tamate, S. (1998). Deformation and failure behaviour of anchored retaining wall induced by excessive excavation in centrifuge model tests. Research reports NIIS-RR-97, p.35-46.

掘削に伴う斜面崩壊メカニズムの解明

武蔵工業大学　学　○小板橋　拓馬　日下部　澄音　正　末政　直晃
独立行政法人　産業安全研究所　正会員　Tamrakar　S.B.　伊藤　和也　豊澤　康男

1. はじめに

土砂崩壊発生の誘因は豪雨や地震のような自然現象と建設工事等の人為的なものの 2 種類に分けることができる。後者の人為的な誘因として、斜面の切取り工事において、自然斜面の下方を取り去ることや斜面を急勾配にすることにより、斜面を不安定化させることが挙げられる。建設工事に従事する労働者が被災する労働災害が毎年繰り返し発生し、それらの中には死亡災害あるいは重大災害(一度に 3 人以上が被災する災害を呼ぶ)に至る場合が少なくない。加えて、労働災害が発生するような斜面崩壊では、崩壊発生の前兆現象が明確に現れず、一瞬のうちに土塊の滑動が起こり崩壊に至る場合が多い。そのため、労働者が退避する時間的余裕がなく避難を困難のものとしている。本研究では、試験盛土斜面の崩壊実験（実物大実験）および、その遠心模型実験より、斜面掘削に伴う斜面崩壊メカニズムを解明することを目的としている。本報告では、実物大実験と遠心模型実験の比較結果を報告する。

表-1　盛土の物性値

	含水比 w (%)	湿潤密度 ρ_t (g/cm³)
成田砂 (締固め程度：大)	25.6	1.688
成田砂 (締固め程度：小)	26.1	1.445

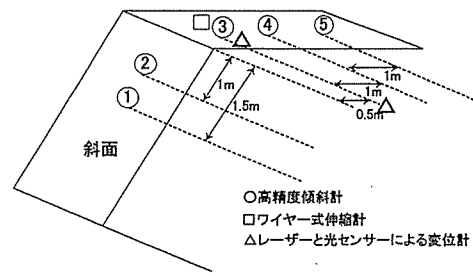

図-1　変位計位置

2. 実物大実験

2. 1概要

宅地造成地域内において実物大実験を行った。実験は、斜面角度50°、高さ5mで切り取った地山（関東ローム）を本体構造とし、腹付盛土の形式で、斜面角度45°、高さ5m となる盛土を作製した。実験に供した盛土材料は現地発生土である成田砂 (ρ_s=2.663g/cm³) である。盛土は、1層の厚さが0.5mとなるようにまき出し、10層に分けて作製した。また、ブルドーザーによる転圧回数により、締め固めの程度を変化させた2種類の盛土を築造した。ここで、盛土の築造後の物性について表－1に示す。それぞれの盛土幅は3.5mであるが、隣の斜面状態を保護する目的で1mの未掘削部を設け、実際の掘削幅を2.5mとして、実験を行った。

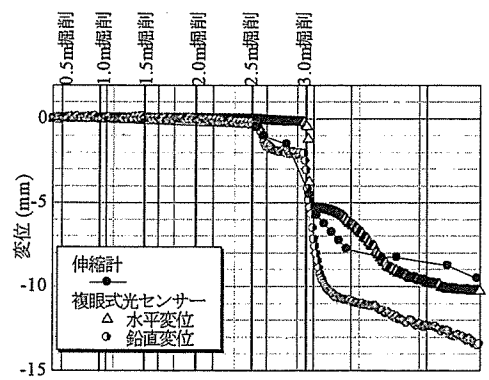

図－2　実物大実験結果

掘削順序は、崩壊したときに他の地盤への影響を防ぐために、弱い地盤であると考えられる転圧回数0回の地盤から行った。掘削は、バックホーにより、1回の切り取り高さを約0.5mとし、最大で7回、高さ約3.5m切り取るという方法を用いた。高さ0.5m切り取るごとに5分間放置し、盛土の変形、傾斜を計測した。試用した計測機器は、ワイヤー式伸縮計、レーザー光と光センサーによる変位計[1)]、高精度傾斜計[2)]であり、図－1の位置にそれぞれ設置した。

2. 2実験結果

本報告では特長的な結果が得られた成田砂（転圧回数0回）の結果について以下に示す。図－2はレーザー光と光センサーによる鉛直方向と水平方向の変位の経時変化を示したものである。切り取り高さ2.5mまではほとんど変化はなかったが2.5mに達したときに部分的な崩壊が生じ、3.0m掘削後に上面で大規模な崩壊が生じた。また、実験後、天端部分に法肩から1.4mと1.9mの位置に、2本のクラックを確認した。

キーワード　斜面安定　遠心模型実験　掘削
連絡先　〒158-8557　東京都世田谷区玉堤 1-28-1　武蔵工業大学　地盤環境工学研究室　ＴＥＬ03-5707-2202

3. 遠心模型実験

3. 1概要

本実験は全て（独）産業安全研究所の所有している遠心模型実験装置にて行った。実物大実験を再現するために、図－3に示すような現場の1/25モデルの模型地盤を作製し、遠心加速度25G場にて実験を行った。使用した試料は、実物大実験にて使用した試料を最大粒径2.0mmに粒度調整したものである。これを現場の含水比、および湿潤密度と等価となるように締め固め圧力を調整し、1層の高さが2cmの地盤を10層に分け、高さ20cm、斜面角度45°の地盤を作製した。また、地盤の底盤部分は地山を想定して、関東ロームを、強い締固め圧力（150kPa）にて圧縮して作製している。掘削には、遠心場掘削装置[3]を用いた。1回の切り取り高さを、実物大実験と等価となるように2cmとし、最大で8回、高さ約16cmの切り取りを行った。遠心模型実験では、高さ2cm切り取るごとに2分間放置し、その間の盛土の変形、傾斜について、接触型変位計、および加速度計により計測した。

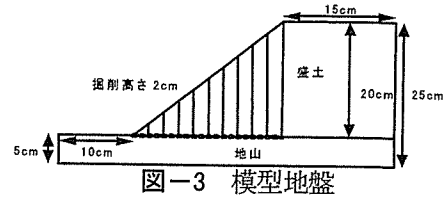

図－3　模型地盤

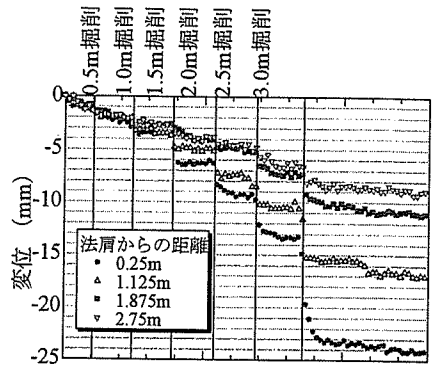

図－4　遠心模型実験結果

3. 2 実験結果

以下の値については、全て実地盤換算で示す。図－4 に接触型変位計から得られた鉛直変位の経時変化を掘削ステップとともに示す。0.5m 掘削から徐々に変位量は増大し、3.0m 掘削後、放置時間中に崩壊に至った。クラックは、法肩から 1.75m の位置にて発生しており、実物大実験でのクラック発生位置に近い傾向が見られた。実験終了後の模型地盤を写真－1 に示す。

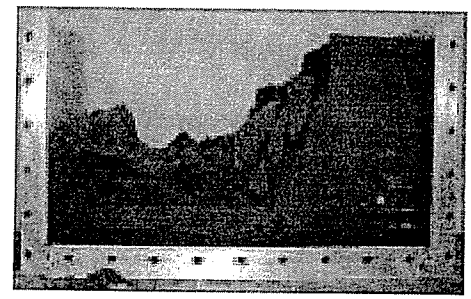
写真－1　崩壊した模型地盤

3. 3 実物大実験との比較

遠心模型実験と実物大実験を鉛直変位から比較する。実物大実験は、法肩から 0.5m の地点に変位計が設置してあるが遠心模型実験では、0.25m、1.125m、1.875m、2.75m に設置した。そこで、0.25m と 1.125m 間は線形に変位していると仮定して 0.5m 地点の変位を換算した。図－5 は、実物大実験、遠心模型実験の各ステップの変位量⊿h をプロットしたものである。初期のステップでは、実物大実験では、ほとんど変位が見られないのに対して、遠心模型実験では、段階に応じて変位が見られる。そして、崩壊するステップに近づくにつれ、両者の変位量は等しくなってくることが分かる。この様に初期状態では変位量が一致しない原因として、側面の境界条件が考えられる。すなわち、実物大実験では、盛土築造に際して端部は異なる実験盛土であり、側面の境界条件は“粗”である。一方、遠心模型実験では、視覚的な把握や現象を単純化するために、土槽側面に貼付したメンブレンとグリスにより、側面の摩擦力を除去し、境界条件は、“滑”としている。このような境界条件の違いが、両者の崩壊形状と共に変位量に影響を与えたものと推察される。

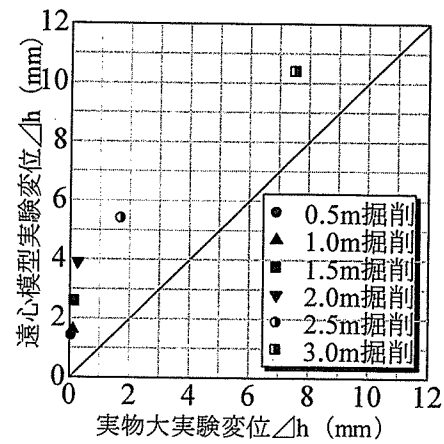

図－5　鉛直変位量比較

4. まとめ

遠心模型実験により、実物大実験を再現した。遠心模型実験結果と実物大実験結果の比較から、切り取り高さ 3.0m 掘削後に崩壊が生じ、斜面の天端部分にクラックが発生したことが一致した。今後、実物大実験を正確に再現するために三次元的な崩壊、側面の境界条件について考慮し、遠心模型実験を行う予定である。

参考文献 1) 伊藤ら「レーザー光と光センサーを利用した土砂崩壊検知システムの開発」、第 44 回日本地すべり学会研究発表会講演集,pp.369-372 ,2005, 2) タムラカルら、「実大実験による法尻掘削に起因する斜面崩壊の前兆現象の検討」、第３５回安全工学シンポジウム,pp. 319-322 2005, 3) S.B.Tamrakar et.al, failure mechanism of slopes in the centrifuge using in-flight excavator, international symposium landslide hazard in orogenic zone from the himalaya to island arc in asia pp.259

掘削に伴う斜面崩壊メカニズムの解明（数値解析を用いて）

武蔵工業大学　学○日下部　澄音　小板橋　拓馬　正　末政　直晃
独立行政法人産業安全研究所　正　伊藤　和也　Tamrakar Surendra B.　豊澤　康男

1．はじめに

道路拡幅工事や急傾斜地対策工事では、従来よりも斜面の勾配を急にし、そこに重力壁等を設置し斜面を安定にすることが多くある。これらの構造物は最終的には斜面を安定化させることができるが、その設置過程においては斜面が不安定化し、崩壊に至ることもある。図-1 に示すように、近年の建設業における死亡者数は減少してはいるものの、土砂崩壊による死亡者は減少していない[1]。このような災害を防ぐためには、斜面の掘削における斜面崩壊メカニズムを解明し、安全な対策工法を提案する必要がある。本研究では、実物大実験、遠心模型実験、数値解析を行った。

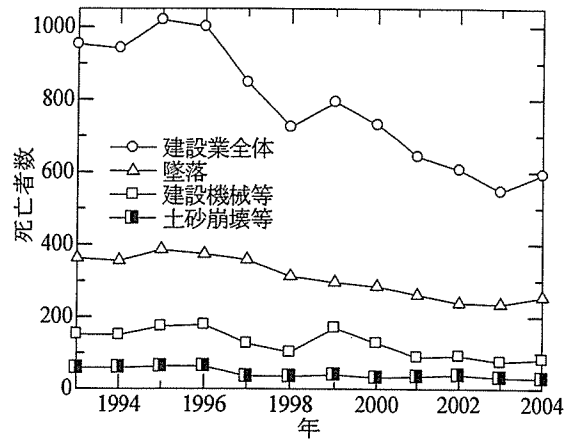

図-1　死亡者数の経年変化[1]

本報告では実物大実験を再現した地盤について数値解析を行い、小板橋ら[2]の報告にある遠心模型実験の結果と比較した。

2．数値解析

2．1　概要

数値解析には有限要素法を用いた地盤の変形解析を行うことのできる PLAXIS[3]を用いた。斜面掘削時における天端の鉛直変位と地盤の塑性化領域について報告する。地盤は実物大実験のサイズとし、本体構造物である関東ロームの地山とその前方に築造された成田砂の腹付盛土から成る。表-1 に解析条件とそれぞれの試料についての入力パラメータ、図-2 に解析対象地盤のサイズをそれぞれ示す。図中の 1～6 は掘削段階（一回につき高さ 0.5m）を表している。解析パラメータである成田砂の湿潤重量には実物大実験時に現地で測定したもの、また、粘着力とせん断抵抗角には実物大実験で使用した試料の圧密定体積一面せん断試験により求めた値を使用している。

表-1　解析条件とパラメータ

材料モデル	モール・クーロン	地山	盛土
特性のタイプ	非排水	関東ローム	成田砂
湿潤重量 γ_t (kN/m^3)		16	15.4
水平方向透水係数 k_x (m/day)		0.02066	0.03267
鉛直方向透水係数 k_y (m/day)		0.02066	0.03267
ヤング率 E_{ref} (kN/m^2)		25000	3000
ポアソン比 ν		0.35	0.35
粘着力 c_{ref} (kN/m^2)		5.2	22.6
せん断抵抗角 ϕ		38.7	10.4

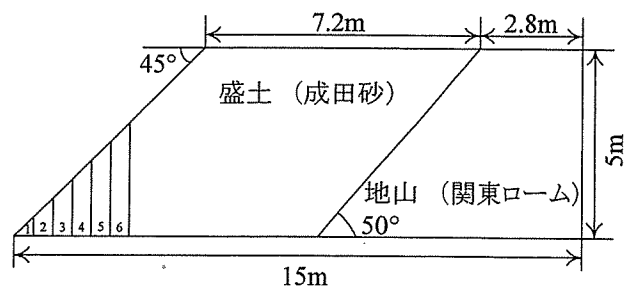

図-2　解析対象地盤のサイズ

2．2　結果の比較と考察

以下に現れる値は全て実物大換算してある。図-3 に遠心模型実験における天端の鉛直変位と時間の関係を示す。これは接触型変位計により計測されたデータであり、法肩から 0.250、1.125、1.875、2.750m の位置に設置し掘削に伴う天端の鉛直変位を計測したものである。なお、図中の垂線は掘削の段階を示している。これ

キーワード　斜面安定　数値解析　掘削

連絡先　〒158-8557　東京都世田谷区玉堤 1-28-1　武蔵工業大学　地盤環境工学研究室　TEL 03-5707-2202

によると法肩に近い変位計ほど大きな変位を計測しており、6回目の掘削により崩壊が生じている。この際、法肩に最も近い変位計が計測したのは約25mmの変位量である。図-4に数値解析を用いて同じ掘削を再現した場合の天端の鉛直変位と計算ステップの関係を示す。法肩から0.210mでの鉛直変位は最大で約16mmであり、遠心模型実験におけるそれと非常に近い値を得ることができた。図-3同様に、垂線が掘削の段階を示しているが、これらからは、1回目の掘削の後、変位は直線から曲線へと変化しているために、ここで地盤が塑性化し始めたのではないかと考えられる。その後緩やかに変位が増加していくが、図中に示すように、3回目と5回目の掘削後変位が大きく変化する箇所がある。これらの箇所において、地盤内部の応力状態を確かめた。図-5と6はそれぞれ3回目と6回目の掘削における塑性化領域と引張応力を持つ領域を示している。掘削面の底部の丸で囲んだ部分は塑性化した箇所を、また天端上部から斜面にかけての黒色の部分は引張応力を持つ領域を示している。塑性領域については、いずれの場合も掘削面底部から斜面上方に向かっていることより、斜面崩壊は斜面底部が塑性化することで発生することと考えられる。また引張応力を持つ領域については、いずれの掘削段階においてもこれが天端部分に広く分布していることより、盛土は掘削に伴ってせん断破壊のみならず、引張破壊によって崩壊する可能性もあると分かる。さらには腹付盛土の天端の大部分においてクラック発生の危険性があることも分かる。

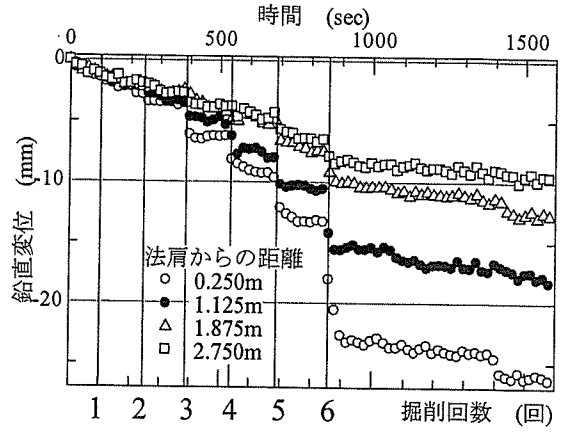

図-3 鉛直変位-時間関係
(遠心模型実験)

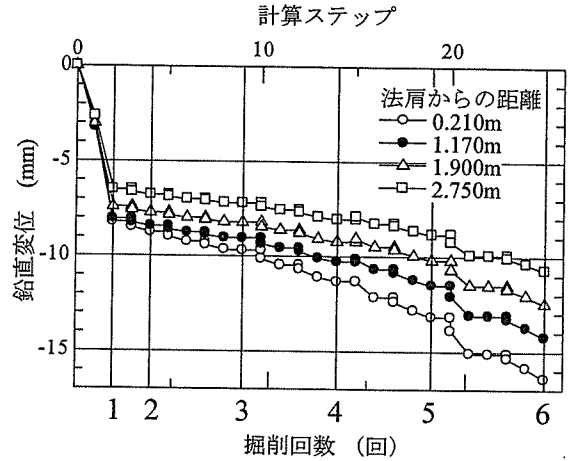

図-4 鉛直変位-計算ステップ関係
(数値解析)

3. まとめ

掘削に伴う斜面崩壊メカニズムを解明するために行った、実物大実験、遠心模型実験、数値解析より以下の知見を得た。

斜面崩壊は掘削面底部の塑性化により発生する。また、崩壊はせん断破壊のみならず、引張破壊でも生じる可能性があり、クラックの発生は天端のいずれの部分にも起こり得ることと考えられる。遠心模型実験との整合性は良く、鉛直変位に多少の違いはあるものの、鉛直変位の傾きや、5回目の掘削後に大きな鉛直変位が起こるという点が一致している。

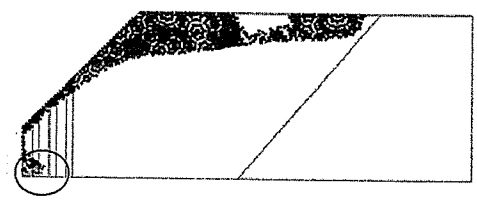
図-5 3回目掘削後の塑性領域と引張応力発生領域

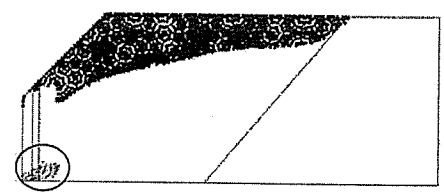
図-6 5回目掘削後の塑性領域と引張応力発生領域

参考文献

1) 建設業労働災害防止協会: 労働災害データ、http://www.kensaibou.or.jp/index.html

2) 小板橋ら: 掘削に伴う斜面崩壊メカニズムの解明、第33回土木学会関東支部技術研究発表会(投稿中)

3) R.B.J.Brinkgreve et.al : PLAXIS 2D-version 8, Delft University of Technology & PLAXIS b.v., The Netherlands

Development of Tilt-sensor for advance prediction of failure and its applicability in the field excavation

Ọ Tamrakar S.B., Toyosawa Y. and Itoh K. (Japan National Institute of Occupational Safety and Health)

1. Introduction

Main purpose of this report is to develop some kinds of measuring instrument, which could measure the slope movement in the real excavating field with which the pattern of failure could be predicted in advance. In this report, in reference to the tilt sensors developed by Tamrakar et al. (2005), two new types; small size compact (SSC) and large size stand alone (SA) were developed and their applicability in the real excavating field was explained. Four types of model slopes were prepared from two types of soils; Narita sand and Kanto loam by compacting each type to Low (L) and High (H) density. Excavation at the toe of the slope was continued at certain interval until the failure occurred. Both types of tilt sensors were set up both on the slope top and slope surface and measurement was done until the failure. Sharp movement of tilt sensor just before the failure was observed for each slope. Finally, tilt angles measured from above tilt sensors during the excavation of Narita sand (L and H) and Kanto loam (L and H) embankments were made. Also, failure patterns were discussed.

2. Tilt sensor

Tilt-sensor used here consists of highly sensitive accelerometers which could measure the tilting angle in the range of ±20° with the sensitivity of 100mV/deg and have thermal sensitivity of 10mV/°C. Both positive and negative angles along both X and Y directions could be measured as shown in Photo 1. Depending upon the requirement of measurement of tilting angle (X and Y directions) and temperature variation, one set of tilt sensor is provided with one, two or three accelerometers. Photo 1 shows the general outline of the tilt sensor used by Tamrakar et. al (2005). In Photo 2, two new tilt sensors; small size compact (SSC) and stand alone (SA) developed to use in the excavation field are shown. It is to be mentioned that SSC is small, simple and compact whereas SA is large and robust. Inner structure of SSC tilt sensor is similar to that shown in Photo 1 which comprises of two accelerometers (X and Y directions). SA tilt sensor comprises of three accelerometers (X, Y directions and temperature). In case of SSC, accelerometers are placed in layers above the base plate whereas in case of SA, accelerometers are directly placed on the base plate. Base plates of SSC and SA sensors are further supported by either flat plate (Photo 2(a)) or tubular pipe (Photo 2(b)). Both of these sensors are directly set up on the slope top and slope surface.

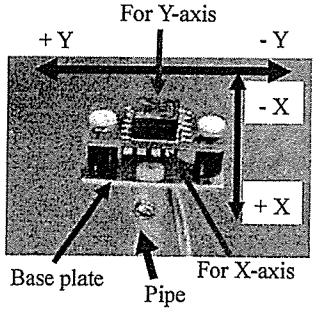

Photo 1 Tilt sensor.

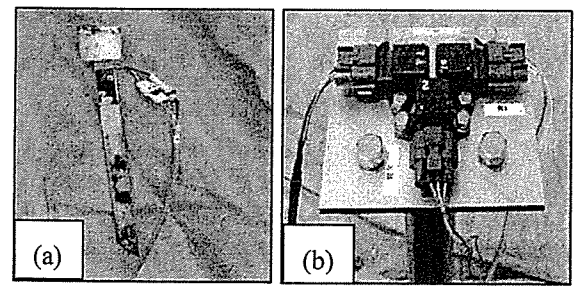

Photo 2 (a) SSC and (b) SA tilt sensors.

3 Tilt sensors set up and Field Test

Four model slopes were prepared from Narita sand and Kanto loam by compaction them with a small size bull dozer. Properties of each soil are shown in Table 1. For each type of soil, two model slopes with two types of densities; high (H) and low (L) were prepared. The height, width and slope angle of the model slope were 5m, 3.5m and 45°, respectively. At 2.5m and 5 m

height, density and water content were measured by two methods; Sand replacement and Core cutter. Average unit weight and water content for each model slopes are shown in Table 2.

Table 1. Properties of soil specimens.

	Narita Sand	Kanto loam
Unit weight of soil solid (kN/m^3)	26.12	27.13
Liquid limit, w_L (%)		129.3
Plastic limit, w_P (%)		91.2
Plasticity index, Ip		38.1
$0.075x10^{-3}$~$2x10^{-3}$m (%)	77.5	11.5
$0.005x10^{-3}$~$0.075x10^{-3}$m (%)	12.7	54.7
<$0.005x10^{-3}$m (%)	9.8	33.8
Avg. particle size, D_{50} ($x10^{-3}$m)	0.1909	0.0119
Soil classification	**SF**	**VH_2-S**

Table 2. Density and water content

Method	Type	Narita Sand		Kanto loam	
		w	unit wt.	w	unit wt.
		(%)	(kN/m^3)	(%)	(kN/m^3)
Sand replacement	Low	29.35	16.4	116.35	10.56
	High	27.45	17.09	111.25	11.62
Core cutter	Low	28.75	15.03	116.4	11.33
	High	28.75	16.16	112.6	11.65

Four SSC (SSC1, SSC2, SSC3 and SSC5) and five SA (SA1, SA2, SA3, SA4 and SA5) type tilt sensors were set up both on the slope and slope top as shown in Fig. 1. Slope surface was divided into 10 equal widths and excavation was started from the toe of the slope, vertically downward using a backhoe. Height and width of each cut were therefore change by 0.5m. About 5 minutes waiting time was allowed between each cut. Toe excavation was continued until full failure of the slope was occurred. Directions of movement of tilt sensor on the model slope are also shown in Fig. 1.

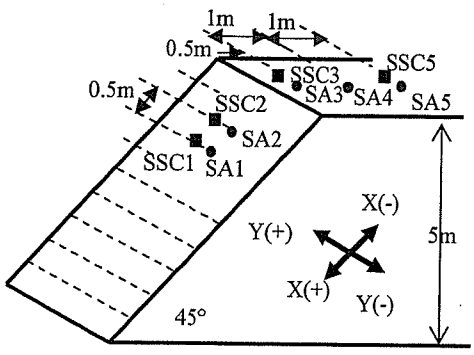

Fig. 1 Layout of slope and tilt sensor set.

In case of Narita sand (L) total of 6 cuts were made. Partial failure was observed after the 5th cut with longer waiting interval. Final large failure was seen after 6th cut at around 40.5 min. elapsed time. Similarly, for Narita sand (H), total of 6 cuts were made and here also, partial failure was observed after 5 cut. But the final failure was observed after 6^{th} cut at around 51 min. elapsed time.

For Kanto loam (L), large partial failure within the slope was seen after 7^{th} cut where SSC1, SSC2, SA1 and SA2 measurements became discontinuous, showing the partial failure reaching around those positions. Then 3 under-cuttings from 51~52.2 minutes were made to see the failure pattern. Movement of the crest of the slope was seen from SSC3 and SA3 tilt sensors with continuous increase in tilting angle measurement and it stopped at around 70 min. elapsed time. In case of Kanto loam (H), total of 9 cuts were made. First partial failure took place after 8 cut at the right side of the slope (right wall). Large change in tilt angle was observed during this partial failure which stopped at around 88 min. elapsed time. Further excavation on the left side of the slope was made and final failure was occurred around 135 min. elapsed time where the failure reached up to SA3 (SSC3) position on the slope crest. During the excavations, tensile cracks were appeared on the slope top in all the cases.

3. Test Results

In this report movements of SSC and SA tilt sensors along the X-direction placed on the slope surface and slope top are only shown. In all the figures, solid lines represent the end excavation for each step. Dotted line at the end shows the final failure time whereas those in between show the occurrance of partial failure except those dotted lines around 51~52.2 min. of Kanto loam (L) which were the under-cutting steps.

Figures 2 and 3 show the movement of SA and SSC tilt sensors measured along X-direction for Narita sand (L). Although it is difficult to see the amount of

movement for the first few cuts, increment in the slope movement with the progress of cut could be seen in all the sensors. Sudden increment in tilt angle measurement could be seen after 5 and 6 cuts. Comparing the movement of SA and SSC placed at the same position, similar trend of movements could be seen. Here, all the tilt sensors moved along the positive X-direction only. Although, movements of SA and SSC along the Y-direction were not shown here, all the Y-direction movements were in the negative direction. This shows the movement of whole the slope in the front and left side of the slope face.

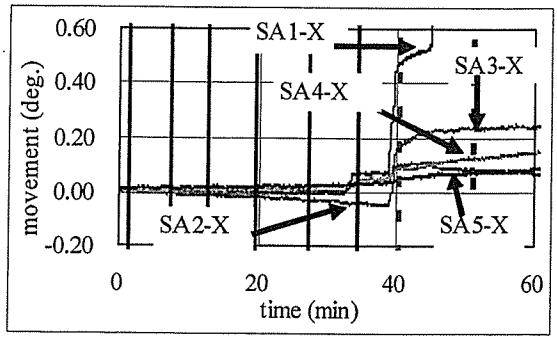

Fig. 2 Movement of SA for Narita sand (L).

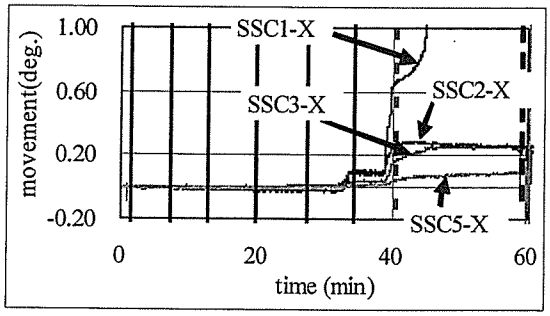

Fig. 3 Movement of SSC for Narita sand (L).

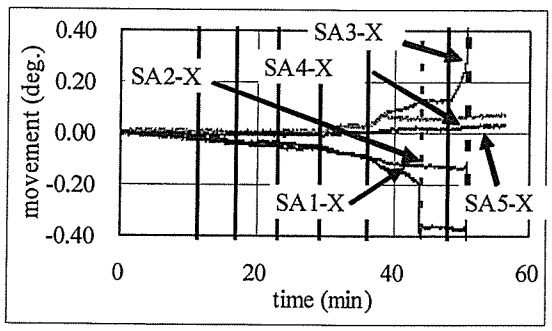

Fig. 4 Movement of SA for Narita sand (H).

In Fig. 4, movements of SA tilt sensors for Narita sand (H) are shown. Here also, sudden increment in the tilt angle was seen after 5 and 6 cuts. Partial failure was stopped after 44 min. elapsed time and then final failure of whole slope took place at 51 min. elapsed time. In contrary to those of Narita sand (L), here all the tilt sensors placed on the slope surface moved in opposite direction to those placed on the slope top. Movements of SSC tilt sensor along Y-direction were negative (not shown). This shows the failure of slope for Narita sand (H) towards the left side of slope face by overturning of upper section of slope (slope crest).

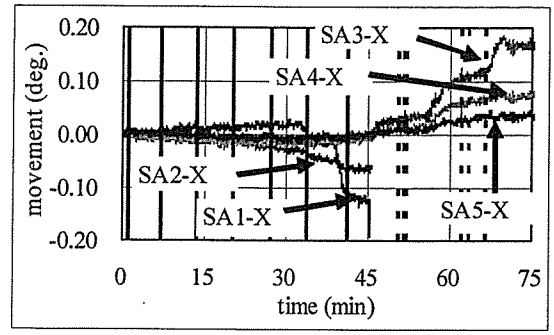

Fig. 5 Movement of SA for Kanto loam (L).

Figure 5 show the movements of SA tilt sensors along X direction for Kanto loam (L). SA1 and SA2 tilt sensors placed on the slope surface were out of order after 7th cut. Increment in the slope sensors took place after 3 under-cuttings made on the toe portion of slope. With partial failure, increment on the tilt sensor movement could be seen. Slope top tilt sensors showed positive X-direction. Movements of SSC tilt sensors (not shown) also showed the similar trend of movement as those by SA tilt sensors. Almost no movement was seen along Y-direction for all tilt sensors. Since the movement of tilt sensors placed on the slope surface could not be used after 7th cut, it is little difficult to trace the failure pattern of whole slope in this case.

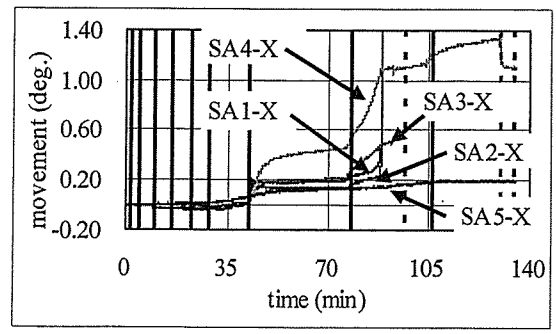

Fig. 6 Movement of SA for Kanto loam (H).

Movements of SA tilt sensors along X-direction for Kanto loam (H) are shown in Fig. 6. Sudden increment in the tilt angle was seen after 7th, 8th and 9th cut. After 7th and 8th cuts, two partial failures were observed. Positive movements along X-directions were seen for all the SA sensors. No movement along the Y-direction was found (not shown). Similar movement along both directions for SSC tilt sensors were found (not shown). This shows the movement of whole slope in the forward and outward from the slope face. This means that whole the slope during failure moved outward and downward from the slope face.

As explained in above, from the X and Y direction movements of tilt sensors, it is possible to predict the failure pattern of slope. In Fig. 7, failure pattern for Narita sand (H) and Kanto loam (H) are shown along with the direction of movement of tilt sensors placed on the slope surface and slope top. Changes in the tilt angle for each SA and SSC tilt sensor along X-direction at particular elapsed time for Narita sand (H) and Kanto loam (H) are shown in Table 1. By comparing the amount of change in the tilt angle, it was seen that Kanto loam (H) showed larger movement and took longer time to fail than that by Narita sand (H) despite

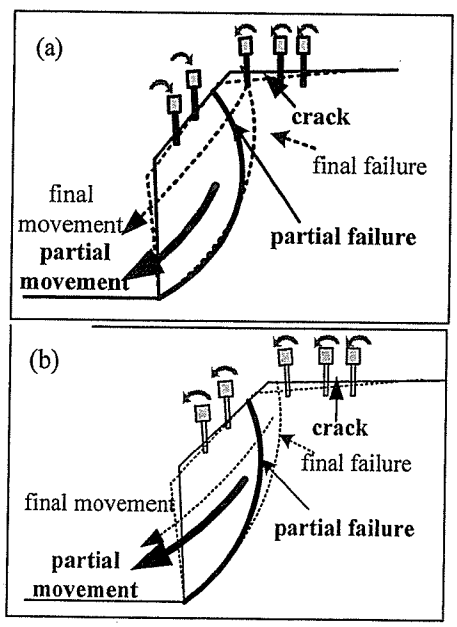

Fig. 7 Failure pattern in two types of soil models (a) Narita sand (H) and (b) Kanto loam (H).

Table 3 Ttilt angles measured along X-axis

Narita sand (H) (around 51 min. elapsed time)					
tilt-angle	1	2	3	4	5
SSC	-0.275	-0.11	0.25	-	0.025
SA	-0.300	-0.15	0.25	0.06	0.025
Kanto loam (H) (around 88 min. elapsed time)					
tilt angle	1	2	3	4	5
SSC	0.50	0.08	0.54	-	0.400
SA	0.50	0.30	0.50	1.08	0.150

of wet density of Narita sand (H) being higher than that of Kanto loam (H). This might be due to the difference in the effect of cohesion and angle of frictional resistance. Also, comparison between SSC and SA type tilt sensors for each soil are also made. Both SSC and SA tilt sensors showed almost same value. This shows the applicability of both types of tilt sensors in the field with equal efficiency. Little variation in SA and SSC tilt sensors for Kanto loam might have occurred due to the size of accelerometers, insertion depth, etc.

4. Conclusions

1) All types of tilt sensors gave good response during the excavation and just before the failure. They showed sharp increment just before the failure. Hence all types of sensors could be used to predict the failure movement during the excavation works.

2) Both SA and SSC tilt sensors used in each model slope showed almost same pattern and same amount of movement. This suggests that both SA and SSC tilt sensors could be used with equal efficiency in the field.

3) Determination of direction of resultant failure movement and failure pattern are possible with these new tilt sensors.

5. Acknowledgement

This work is partially carried out under the Health and Labor Sciences Research Grants of Ministry of Health, Labor and Welfare.

References

Tamrakar S.B., Toyosawa Y., Itoh K. and Ariki T.:「実大実験による法尻掘削に起因する斜面崩壊の前兆現象の検討」, 第３５回安全工学シンポジウム、pp. 319-322 (2005).

Relationship between critical failure height and trench excavation depth in relation to centrifuge tests performed with In-flight excavator

O□ Tamrakar S.B., Toyosawa Y., Itoh K. and Timpong S. (Japan National Institute of Occupational Safety and Health)

1. Introduction

Most of the accidents take place during the excavation of lower parts of the slopes, especially the trenches (excavation below the toe level). Earlier Tamrakar et. al (2005) carried out the tests at centrifuge using in-flight excavator for volcanic sand with and without making trench excavations at the beginning and it was reported that the vertical height before the failure was larger for the excavation made without trench at the start of trench excavation than the excavation made with the trench. In this research, trench excavations are made at different distances from the toe of the slope along with the normal excavation and the effect of trench excavation on the failure height just before the failure was studied. Comparison of failure heights observed for the normal and combined excavations is made. With this, a better and safer position of trench excavation could be made. Also, stepwise sharp increment in displacement during the excavation and just before the failure with linear vertical differential transducer (LVDT) set up on the slope crest showed the possibility of prediction of failure in advance.

2. Preparation of Model Slope and Set Up

In this experiment, Narita sand collected from the Toke excavation site, Chiba prefecture, Japan was used. Physical properties, particle size distribution and direct shear test results of this soil is shown in Table 1. Soil specimen was thoroughly mixed with pre-determined water content (w) and kept in plastic bag for several days. Model slope ground from these soils was prepared in a model box (0.45 m x 0.20 m x 0.272 m), by statically compacting them into number of layers using bellofragm cylinder under 50 kPa. Thickness of each layer is about 0.02 m and compaction time for each layer was about 5 minutes. Model slope ground was then cut into required dimensions shown in Fig. 1 with fixed slope angle of 50 degree. This slope angle is lower than the one mentioned in the safety guideline of Labor Safety and Health Regulation. The lower and safer angle was selected so that longer slope length (i.e. distance of excavation from the toe of the slope) could be obtained which will facilitate to make trench excavations at different distances from the toe. Completed model slope along with model box was finally shifted to centrifuge platform. Direct contact type LVDT (D-1 to D-5) were placed on the top surface of the slope at 0.01, 0.04, 0.07, 0.105 and 0.142 m distances from the crest of the slope (Fig. 1). Once the set up of LVDT was finished, in-flight excavator (Toyosawa et. al, 1998) was positioned in the centrifuge platform in such a way that its blade could

Table 1. Properties of Narita sand

	Narita Sand
Unit weight of soil solid (kN/m^3)	26.12
0.075x10^{-3}~2x10^{-3}m (%)	77.5
0.005x10^{-3}~0.075x10^{-3}m (%)	12.7
<0.005x10^{-3}m (%)	9.8
Avg. particle size, D_{50} (x10^{-3}m)	0.1909
Soil classification	SF
Cohesion, c (kPa)	9.78
Angle of internal friction (ϕ°)	15.88

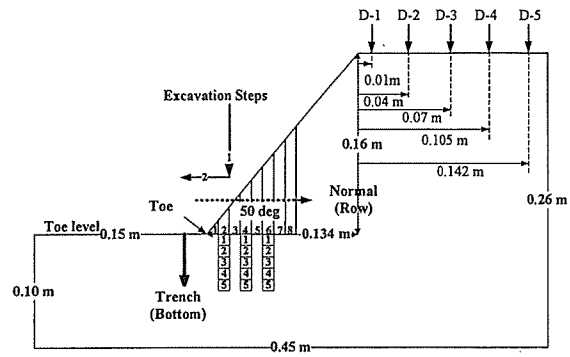

Fig. 1 Outline of model slope showing the positions of LVDTs on the slope top.

move freely within the model box.

3. Details of Centrifuge Model Tests

Experimental conditions for one normal and three combined excavations (normal + trench) are shown in Table 2. Each excavation (cut) was carried out vertically downward and outward from the slop.

In case of normal excavation, cutting was started from the slope surface to vertically downward and up to toe level. Width of each vertical cut of the model slope in normal excavation is 0.01 m. Each vertical cut (above the toe level) is represented by "Row (R)" and it is followed by the numbers as follows; R-1, R-2, R-3 and so on. R-1 represents the 1st cut, excavating at 0.01 m distance from the toe of the model slope. Similarly, R-2 and R-3 represent the second and third cuts, excavating the model slope at 0.02 and 0.03 m distances from the model slope toe, respectively. Combined excavation represents the trench excavation at particular normal cut (row). Trench excavation represents the vertical cut behind and below the toe level at particular Row (R). Depth of each cut of trench of model is fixed at 0.01 m and trench excavation is represented by "Bottom (B)" which is followed by numbers as follows; B-1, B-2, B-3, and so on. B-1 represents the cut at 0.01 m below from the toe level. Similarly, B-2 and B-3 represent the cuts at 0.02 and 0.03 m depths from the model slope toe level, respectively. During the normal excavation, model slope was failed at R-8-B-0. Hence combined excavations were carried within the range from the toe to this failure distance. Here, R-2, R-4 and R-6 were chosen to carry out the combined excavations. Each case of excavation is shown in Table 2. For example: R-2-B-5. This represents the width of normal cut behind and at the toe level is 0.02 m (i.e. at 0.02 m distance from the model slope toe) and depth of trench cut behind and below the toe level is 0.05 m; showing the excavation at 0.02 m distance from the toe and up to 0.05 m depth below the toe level.

Table 2. Experimental conditions for Narita Sand.

Type of excavation	Normal	Combined		
Cases	R8-B0	R2-B5	R4-B3	R6-B2
Bulk unit wt. (kN/m^3)	10.94	12.56	12.18	12.7
w (%)	9.89	10.75	9.22	9.22
Acceleration, G	31.3	31.3	31.6	31.8
Failure ht. (R) (m)	2.985	0.746	1.507	2.275
Failure depth (B) (m)	0	1.565	0.948	0.636
Critical failure ht. (m	2.985	2.311	2.455	2.911
H_{cr} (m)	3.576	3.115	3.211	3.079

In this research, height of the slope in the field from the toe level was assumed to be 5 m. But the slope height (height from the toe level to slope top) was 0.16 m (total height of the model is 0.26 m). Therefore to meet the slope height of 5 m, centrifuge acceleration was increased up to 31.3 G. Similarly, for other cases also acceleration was fixed in such a way that their real slope height becomes 5 m. Accelerations for each case are shown in Table 2. During the test, acceleration was increased gradually in steps from 5 ~ 10 ~ 15 ~ 20 ~ 25 ~ 31.3G. Once the vertical displacement become constant at 31.3G, then the excavation was started.

4. Test Results and Discussions

Excavation test results are shown in Table 2. In the table, all the values are changed into real field value by multiplying the data obtained from model test by the respective centrifuge acceleration values. 'Failure height' in table represents the height of slope above the toe level just before the failure. Similarly, 'Failure depth' represents the depth of trench cut below the toe level. 'Critical failure height' represents the summation of failure height and failure depth. Critical failure height is the maximum for normal cases and it reduces with the combined excavation near the toe. 'Critical height $[H_{cr}=(4*c)/\gamma_t]$)' shown in the Table 2 was calculated theoretically by using the equation where bulk unit weight and cohesion are used. Critical failure height obtained from the normal and combined excavation cases was smaller than those calculated theoretically. As theoretically obtained critical value is larger than those obtained from excavation, one should be careful while using the critical failure height as the reference during the excavation works.

Relationship between failure height (Row) and failure depth (Bottom) just before the failure at particular distances of excavation from the toe is shown in Fig. 3. Excavation position (R-cut) of the model tests was multiplied by the centrifuge acceleration to get the real distance of excavation position from the toe. At particular distance of excavation, failure height is fixed as the slope angle of the model is constant. But as observed from the graph, failure depth decreases with the increase in the distance of excavation. This relationship is non-linear.

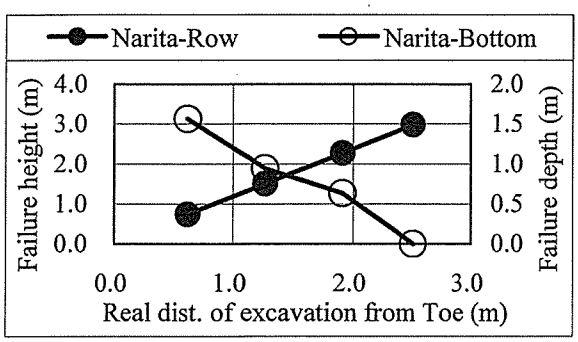

Fig. 3 Relationship between failure height and failure depth with distance of excavation from toe.

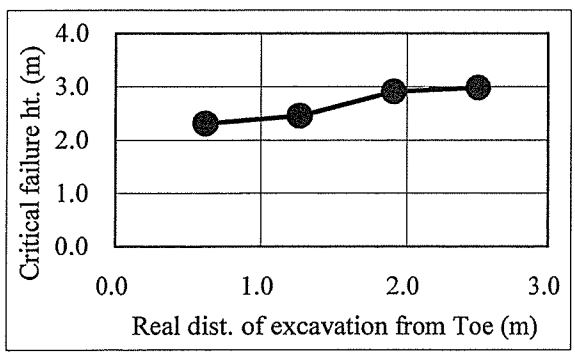

Fig. 4 Relationship between critical failure height and distance of excavation from toe.

Figure 4 shows the relationship between critical failure height and real distance of excavation position from the toe point of the slope. Critical failure height increases with the increase in the distance of excavation position from the toe. But the increment rate decreases with the increase in the excavation distance from the toe, showing the non-linear relationship. This implies that at toe or near the toe, if the trench excavation is to be made, the failure of slope might take place before it reaches the critical failure height obtained either from the normal excavation or from the theoretically calculated critical height. Henceforth, care should be taken while carrying the combined (trench) excavation.

Decrease in the critical failure height with the increase in the failure depth (trench excavation) might be thought of due to the increase in the overburden pressure (weight of extra height) behind the cut. Generally, when the toe of the slope is excavated, shear strain is accumulated near the toe. With the advancement in the combined excavation steps near the toe, overburden pressure continues to increase. Continuous increment in the overburden pressure behind the cut increases the shearing strain which finally leads to failure and slope gets failed. This is the reason why critical failure height near the toe of the slope is smaller than those at farther distances from the toe. Therefore, critical failure height during R2 cut showed the minimum value in comparison to R8 cut where the critical failure height was the maximum. From the results mentioned in Figs. 3 and 4, it could be said that the maximum value of critical failure height could only be obtained for normal excavation cases and this critical failure height decreases with the decrease in the distance of excavation position as well as with the increase in the trench excavation depth.

Figure 5 show the vertical displacement measured from LVDTs set up on the top surface of the slope for normal excavation case (R8-B0). Dashed vertical lines in the graph represent the steps of excavation. Here, elapsed time for each excavation is shown. Thus, finishing time for first step of excavation is at zero minutes. Gradual increase in vertical displacement with the increase in the steps of excavation could be observed. Comparing the amount of vertical displacement of each LVDT (D-1, D-2, D-3, D-4 and D-5), D-1 shows the maximum value and D-5 shows the minimum, D-1 was the displacement just on the crest of the slope. Large and sharp increment of D-1 displacement showed the possibility of prediction of

failure in advance if the measurement is made at the crest of the slope. Comparing the displacement of pattern of all the LVDTs in Fig. 5, it showed that whole slope moved forward and downward with the increase in the excavation steps.

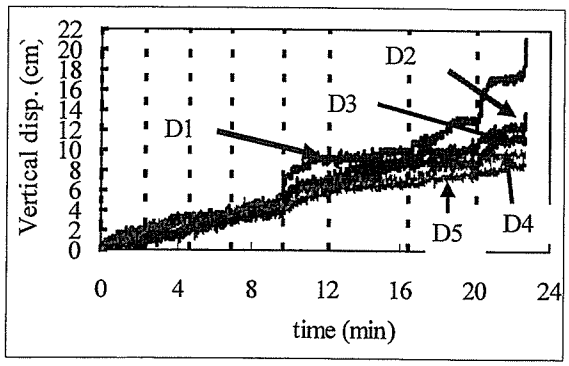

Fig. 5 Relationship between vertical displacement and elapsed time of excavation.

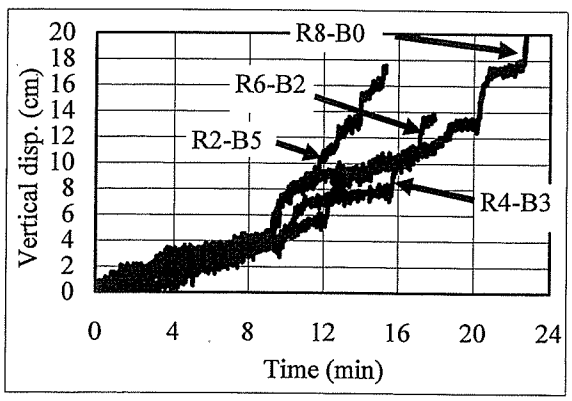

Fig. 6 Vertical displacement of D-1 with time for all the excavation cases.

In Fig. 6, vertical displacement of LVDT (D-1) for all the test cases is shown. Here also, finishing time of 1st cut was at zero elapsed time. Gradual increase in vertical displacement with the increase in the steps of excavation could be observed. Displacement pattern for each excavation cases changed after 9.7 minutes elapsed time (i.e. after 5th cut in normal excavation case). Comparing the failure time, R2-B5 took the minimum time and R8-B0 took the maximum. This shows that normal excavation takes longer time to fail than combined excavations; deeper trench excavation showing the minimum time for failure. Sharp increment in displacement pattern for R2-B5 excavation case also shows the possibility of quicker failure. From these, it could be said that while combined excavations are carried out at the toe, proper care should be taken as the possibility of failure during these excavations are higher than those at farther distances.

5. Conclusions

(1) Maximum critical failure height was obtained for normal excavation. In case of combined excavation, critical failure height (failure height + failure depth) decreases with the increase in the trench excavation depth. Reduction in the critical failure height near and towards the toe is due to the increase in the overburden pressure (weight of extra height) behind the cut.

(2) Gradual increment in vertical displacement measured on the top surface of slope showed the forward and downward movement of the slope. Sharp and maximum increment in vertical displacement of D-1 nearest to the slope crest showed possibility of failure prediction in advance.

(3) Failure time for combined excavation (normal + trench) is smaller than that for normal excavation; combined excavation made nearer to the toe showed the minimum time to fail. Also, displacement pattern nearer to the toe showed sharp increment.

6. Acknowledgement

This work is partially carried out under the Health and Labor Sciences Research Grants of Ministry of Health, Labor and Welfare.

References

1). Tamrakar, S.B., Toyosawa, Y., Itoh, K. & Kusakabe, S. 2005. Failure mechanism of slopes in the centrifuge using In-flight excavator, International symposium on Landslide Hazard in Orogenic Zone from the Himalaya to Island Arc in Asia, Kathmandu, Nepal, 25-26 September 2005: 255-264.

2). Toyosawa, Y., Horii, N., & Tamate, S. 1998. Deformation and failure behavior of anchored retaining wall induced by excessive excavation in centrifuge model tests, Research Reports of the National Institute of Industrial Safety (NIIS-RR-97):35-46.

Slope Failure Mechanism during Trench Excavation in Peat

○ Sahaphol Timpong, Yasuo Toyosawa, S.B. Tamrakar and Kazuya Itoh
(Construction Safety Research Group, Japan National Institute of Occupational Safety and Health)

1. Introduction

During trench excavation, surcharge loads from excavated material stockpiled on the top of slope play the important role on the stability of slope. Due to high compressibility and low shear strength of peat ground, light loading can even result in large deformation and heavy loading can lead to extreme deformation and failure. In this paper, a series of centrifuge modelling test was conducted in order to investigate the mechanism of slope failure during trench excavation in peat ground using the Mark-II centrifuge (2.3 m radius with a maximum acceleration capacity of 100g) at the National Institute of Industrial Safety (NIIS). In general, the centrifuge modelling of slope failure was performed by increasing the acceleration level until the slope failure can be observed (gravity turn-on technique). This technique provides dramatic results and does not require complicated surcharging systems to bring the slope to failure.

2. Model preparation

In this paper, the centrifuge test was performed in a rigid model box with a transparent Plexiglas sidewall to enable side viewing of the model during centrifuge flight. The internal dimensions of the rectangular model box are 150×450×272 mm. It is common to use the same soil in the model test as in the prototype. However, in case of peat ground which contains many different sizes of roots and fibers, it is extremely difficult to use the natural peat in the centrifuge test due to the effect of scaling laws. During the increasing of centrifuge acceleration, the size of fibers and roots will increase by N times of gravity. For example, peat with a 5 mm diameter root tested at the centrifuge acceleration of 50g, the root diameter will become 25 cm corresponding to the prototype scale. In order to overcome this problem, the peat ground model was prepared by mixing the slurry of Kaolin (NSF clay) and a very small size of sawdust (diameter less than 0.1 mm) as a ratio of about 4:3 by weight at 200% water content in the mixing machine. After the mixing, the slurry was placed into the model box and pre-consolidated under a consolidation pressure of about 10 kPa. By this method, relatively high water and organic content, and low density can be achieved in the peat ground model which is consistent well with the natural peat. The resulting block of the peat ground model was trimmed to form the trench geometry. The embankment of excavated material was prepared in another container by static compaction using the bellofram cylinder. The embankment was trimmed to a desired geometry and then placed on the top of the peat ground model. To observe the two-dimensional deformation characteristics such as displacement and strain distributions in the ground model during the centrifuge flight, a number of rivets made of aluminum with a circular flat edge were used as targets. The targets were embedded into the slope model at a horizontal and a vertical spacing of 20 mm. In order to reduce the sidewall friction, silicone grease was smeared between the model and the sidewalls.

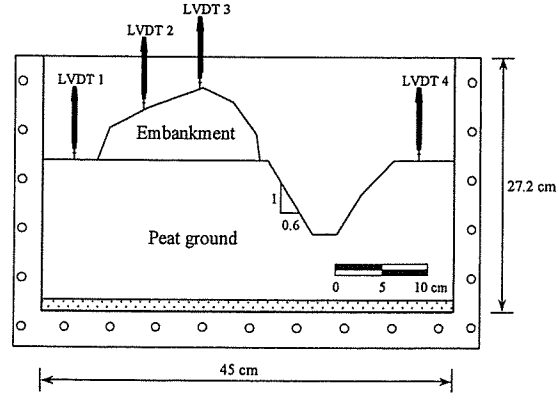

Fig. 1. Schematic view of experimental model